Title

Nonlinear transfer in heated L-modes approaching the L–H transition threshold in Alcator C-Mod

Journal

Nuclear Fusion, 55(8)

ISSN

0029-5515

Authors

Cziegler, I
Tynan, GR
Diamond, PH
et al.

Publication Date

2015-08-01

DOI

10.1088/0029-5515/55/8/083007

Peer reviewed

Nonlinear transfer in heated L-modes approaching the L-H transition threshold in Alcator C-Mod

I Cziegler[1], G R Tynan[1], P H Diamond[1], A E Hubbard[2], J W Hughes[2], J Irby[2], J L Terry[2]

E-mail: iczieglerucsd.edu
[1] University of California San Diego, Center for Momentum Transport and Flow Organization, 9500 Gilman Drive, La Jolla, CA, 92093
[2] Massachusetts Institute of Technology, Plasma Science and Fusion Center, 175 Albany Street, Cambridge, MA, 02139

Abstract. Nonlinear transfer processes between large-scale edge flows and the ambient broadband fluctuations have been shown to play a significant role in the dynamics of edge turbulence, including spreading power from coherent modes and suppressing turbulence at the formation of edge transport barriers. In order to predict thresholds of confinement regimes, both the transition dynamics and the parametric dependence of the nonlinear energy transfer must be studied. Since the expected flow damping terms depend on ion collision rates and local safety factor, recent experiments aimed also to explore the nonlinear drive at various values of the plasma current, density and amount of auxiliary heating. Nonlinear interactions between zonal flows and turbulence in L-mode are estimated using bispectral as well as time-resolved methods based on gas-puff-imaging in Alcator C-Mod[1].

PACS numbers: 52.25.Fi, 52.35.Kt, 52.35.Mw, 52.35.Ra, 52.55.Fa, 52.70.Kz

Accepted for publication in *Nuclear Fusion*

1. Introduction

Through the past decade, a considerable amount of effort has been put toward both experimental studies[2, 3, 4, 5, 6, 7, 8, 9, 10] and modeling[11, 12, 13, 14] of nonlinear transfer mechanisms in magnetically confined plasmas. Most of the resulting works have concentrated on the three-wave coupling mediated spectral transfer of density, energy and vorticity fluctuations. Of these mechanisms, the development and evolution of flow structures on a large spatial scale occupies a special place due to its significant influence on macroscale dynamics, and thus on heat and mass transport across the magnetic field.

The most striking change of these transport processes is no doubt the rapid change from the low- to the high-confinement plasma state[15], or L-H transition. The recent literature of the field has shown an increasing interest in developing a physics based, quantitative model to predict the threshold level of plasma heating power at which the transition occurs for any set of operating parameters. The task is composed of two parts. On the one hand, one needs to understand the microscopic physics of the direct trigger to the transition. However, to predict the L-H transition threshold, it is also necessary to understand the evolution of turbulence nonlinearities in low-confinement (L-mode) plasmas as they approach the transition. Of particular interest is the dependence of these nonlinearities on the amount of cross-field heat flux, which in turn is directly influenced by the auxiliary heating power, plasma current and plasma density.

Recent research has demonstrated the microphysics which leads directly to the L-H transition, both experimentally and in models, as the depletion of turbulence power via nonlinear kinetic energy transfer to zonal flows (ZF). A critical level of transient nonlinearity was determined, and a detailed quantitative comparison of both turbulence suppression and the Reynolds stress mediated nonlinear transfer showed the latter to be more than sufficient to account for the former. While the result established the significance of nonlinear transfer as a turbulence suppression mechanism, the large margin (up to a factor of 50 in some cases) by which transfer exceeded turbulence loss clearly calls for further investigation. The present contribution aims to underpin this argument by resolving the observed discrepancy as far as experimentally possible.

In terms of the parametric dependences of turbulence, progress has been largely experimental. The most relevant result to date[5] addressed the physics of turbulence-ZF interaction in strongly heated L-mode plasmas in a relatively tenuous, limited tokamak plasma without magnetic shaping. In particular, it showed a competition between low-frequency zonal flows [16] and geodesic-acoustic modes (GAM) [17] for the free energy of turbulence, as well as a monotonically increasing trend in the ZF branch against applied heating power. A similar analysis in a strongly shaped plasma with a more reactor relevant design, fine density control and tests of trends against other operating parameters is an absolute necessity for connecting L-mode plasma physics to a more general threshold prediction.

This paper reports the first direct measurements of nonlinear kinetic energy transfer rates in the edge plasma of a high performance, diverted tokamak operating in L-mode. Since in plasmas whose poloidal cross sections exhibit an X-point, the direction of the $\nabla \boldsymbol{B} \times \boldsymbol{B}$ has been known to affect the threshold on auxiliary heating power necessary for accessing high confinement regimes, this represents a crucial step in understanding the route to confinement transitions. Bispectral estimates are presented from several experiments, exploring the dependence of nonlinear energy

transfer on heating power and plasma current, and its effect on the H-mode threshold. The paper also expands on recent results on the L-H transition dynamics by presenting the first completely radially resolved quantitative comparison of turbulence suppression to the nonlinear transfer of kinetic energy.

The paper is organized as follows. Experimental setup and conditions are explained in Section 2. The basic equations which motivate the time-resolved analysis methods are reiterated in Section 3, and the results of this analysis are shown demonstrating the sequence of the L-H transition. Once the onset criteria are established, Section 4 addresses the parametric dependence of the nonlinear energy transfer whose critical value represents the physical threshold in L-mode.

2. Experimental setup

All the experiments reported in this paper were performed on the Alcator C-Mod tokamak[1], a compact ($R_0 = 0.68\,\mathrm{m}, a \simeq 0.21\,\mathrm{m}$) toroidal device with a high magnetic field (up to $B_\phi \leq 8\,\mathrm{T}$, with a typical $B_\phi = 5.4\,\mathrm{T}$). The next sections discuss two types of experiments. Plasmas discussed in Section 3, exhibiting a fully realized L-H transition, were produced with currents of $I_p = 0.8 - 1.0\,\mathrm{MA}$ and magnetic field geometries in an H-mode "favorable" $\nabla \boldsymbol{B} \times \boldsymbol{B}$ direction (i.e. towards the active X-point). L-mode plasmas, shown in Section 4, were produced with currents of $I_p = 0.8 - 1.2\,\mathrm{MA}$ and an H-mode "unfavorable" geometry (i.e. drift away from the active X-point), in lower single null (LSN) geometries. The additional heating that is required for the eventual formation of the temperature pedestal is provided by ion-cyclotron resonance heating (ICRH) with a maximum coupled power of 2.1 MW for these experiments.

The immediate trigger of the L-H transition was determined by focusing on the few millisecond time interval just before and after the transition. Two-dimensional fluctuation data was acquired via gas-puff-imaging (GPI)[18] on the low-field-side midplane of the device. A poloidal section of Alcator C-Mod is shown in Figure 1 with the outboard GPI views overlaid. GPI records fluctuations of the intensity of light emitted by a locally introduced diagnostic neutral gas.

The diagnostic gas puff enters from a nozzle mounted in the limiter, 2.54 cm below the height of the magnetic axis. The GPI viewing array covers a two-dimensional area of considerable size at this location, extending both into the region of closed flux surfaces and into that of open field lines. The viewing area is $3.5\,\mathrm{cm(radial)} \times 3.9\,\mathrm{cm\,(vertical)}$, with an in-focus spot size of 3.8 mm for each of the 9×10 individual channels. All views are coupled to avalanche photodiodes (APD) sampled at 2 MHz. In order to enhance the gas-puff-enhanced-to-background brightness ratio, we used He puffs into D plasmas, therefore the recorded intensities are band-pass filtered for the HeI ($3^3D \rightarrow 2^3P$), $\lambda = 587.6\,\mathrm{nm}$ line. Velocimetry is based on time-delay-estimation (TDE) optimized for the fast 2D APD array[19]. The method, presented in more detail in [10], yields edge plasma velocities at a fast time resolution ($\sim 10\,\mu\mathrm{s}$) with an effective Nyquist frequency of 50 kHz.

3. The L-H transition

Recent experiments performed on Alcator C-Mod[10] have demonstrated the sequence of events directly triggering the L-H transition. Results show that the suppression of turbulence takes place as a lossless nonlinear transfer of kinetic energy from the

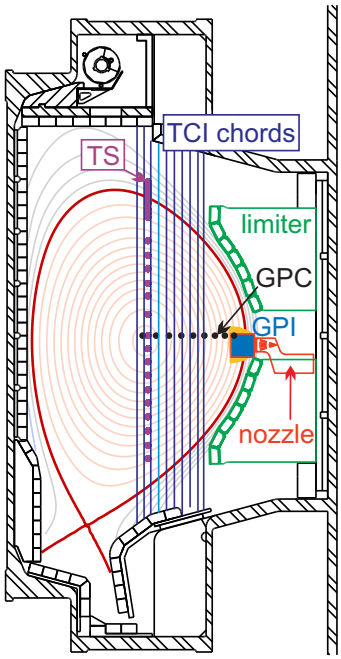

Figure 1. (color online) Configuration of the GPI viewing array (blue square) in a poloidal cross section view with a representative lower single null (LSN) magnetic equilibrium. The solid (red) D-shape curve represents the last closed flux surface (LCFS). The 10 vertical chords of the FTCI are overlaid in blue with the chord whose signals plotted in Figure 2(d) in cyan. Measurement locations of Thomson scattering (solid purple circle) and ECE grating polychromators (GPC, black) are also displayed.

turbulence into radially localized, large spatial scale, slowly evolving components of the velocity fluctuation spectrum, commonly known as zonal flows. Detailed quantitative analysis showed that the normalized amount of kinetic energy converted was consistently quite substantially (up to $\times 50$) larger than the observed reduction in turbulence power, albeit with large error bars on both quantities. While this result is not inconsistent with the nonlinear transfer playing the key role in turbulence suppression, resolving the discrepancy between the above central quantities of the transition is important for making a strong argument.

Here we will briefly recall the analysis method used in demonstrating the above result and the set of equations it is based on, which highlight the connection to the now well-known predator–prey model of edge turbulence[14]. The rest of the section concentrates on refining the quantitative comparison methods involved in evaluating the turbulence nonlinearity.

Starting from the poloidal component of incompressible fluid equations and performing a Reynolds decomposition, a few well-founded assumptions lead to a simple form of the predator–prey model as

$$\partial_t \tilde{K} = \gamma_{\text{eff}} \tilde{K} - P - \partial_r \tilde{T} \tag{1a}$$

$$\partial_t \bar{K} = P - \partial_r \bar{T} - \nu_{\text{LF}} \bar{K} \tag{1b}$$

where we introduced the notations

$$P = \langle \tilde{v}_r \tilde{v}_\theta \rangle \partial_r \langle v_\theta \rangle;$$
$$\tilde{K} = \frac{1}{2}\langle \tilde{v}_\perp^2 \rangle, \quad \tilde{T} = \frac{1}{2}\langle \tilde{v}_r \tilde{v}_\theta^2 \rangle$$
$$\bar{K} = \frac{1}{2}\langle v_\theta \rangle^2, \quad \bar{T} = \langle \tilde{v}_r \tilde{v}_\theta \rangle \langle v_\theta \rangle,$$

similarly to the analysis presented in [7, 11, 20, 21, 22]. The mean in the definition of the Reynolds stress can be understood as either temporal or spatial averaging. Since the paper is focused on slowly evolving zonal flows, $\langle . \rangle$ will represent *both* a time averaging and a poloidal averaging of the available spatio-temporal data. As in Ref. [22], we refer to P as the zonal flow production term, and note that $P - \partial_r \bar{T}$ represents the Reynolds work, while the total loss of local turbulent kinetic energy due to nonlinearity is $P + \partial_r \tilde{T}$, where $\partial_r \tilde{T}$ is turbulence spreading. By balancing the terms on the RHS of $(1a)$, one obtains the condition for the onset of rapid turbulence suppression:

$$R_T \equiv \frac{P + \partial_r \tilde{T}}{\gamma_{\rm eff} \tilde{K}} > 1 \tag{2}$$

meaning that there is enough energy transfer into the zonal flow to overcome the turbulence drive. Here we introduced the dimensionless production parameter, denoted as R_T, in order to match the convention of recent publications [23] The dynamic variables in this condition are directly measured, while the effective growth rate of the turbulence is estimated from $(1a)$ itself using data obtained in regular, time-stationary L-mode as $\gamma_{\rm eff} = \left[(P + \partial_r \tilde{T})/\tilde{K}\right]$.

Figure 2 shows the evolution of a typical L-H transition in Alcator C-Mod at the location of maximal nonlinear transfer, $r_{\rm LCFS} - r = 0.7\,$cm inside the separatrix. The time history of the normalized production parameter R_T is highlighted at the top of the figure. The turbulent kinetic energy $\tilde{K}$ changes are consistent with previous observations. As shown in reported experiments, turbulence suppression occurs when R_T surpasses the threshold, marked by the blue dashed line in the graph. This trigger often follows a short transient increase in turbulence, Figure 2(b), which then leads to a stronger zonal flow drive, which in turn pushes the plasma over the threshold. The fastest acceleration in the zonal flow, Figure 2(c), occurs very near the time when R_T peaks, and as expected, when turbulence power decreases most rapidly too. The first 1 ms of the increasing trend in line integrated density has been shown to correspond to the formation of the pedestal, which takes place just as the turbulence reaches its lowest amplitude, marked by the orange dashed line in Figure 2(d). As the zonal flow is nonlinearly driven by the turbulence, when turbulence is suppressed, the flow is damped out through collisional effects. If, as in Figure 2(e), the pressure gradient grows sufficiently strong during this time, the turbulent transport stays weak due to the well-known pressure gradient induced radial electric field shear.

Given the short time span of the excursion in R_T, the total transferred power was previously estimated from R_T and compared to the loss of turbulence as a consistency check, that is, to confirm the nonlinear interaction as the primary cause of the transition. For this quantitative test, we note that $\gamma_{\rm eff}$ is not expected to vary until the edge gradients are significantly increased in the transition. Thus the test was formulated from the model equation as comparing the two dimensionless integrals $\ln\left(\tilde{K}_{\rm L}/\tilde{K}_{\rm m}\right)$ to $\int_{t_0}^{t_m}(R_T - 1)\gamma_{\rm eff}\,{\rm d}t$, with $\tilde{K}_{\rm m} = \tilde{K}(t_{\rm m})$ is the amount of turbulence

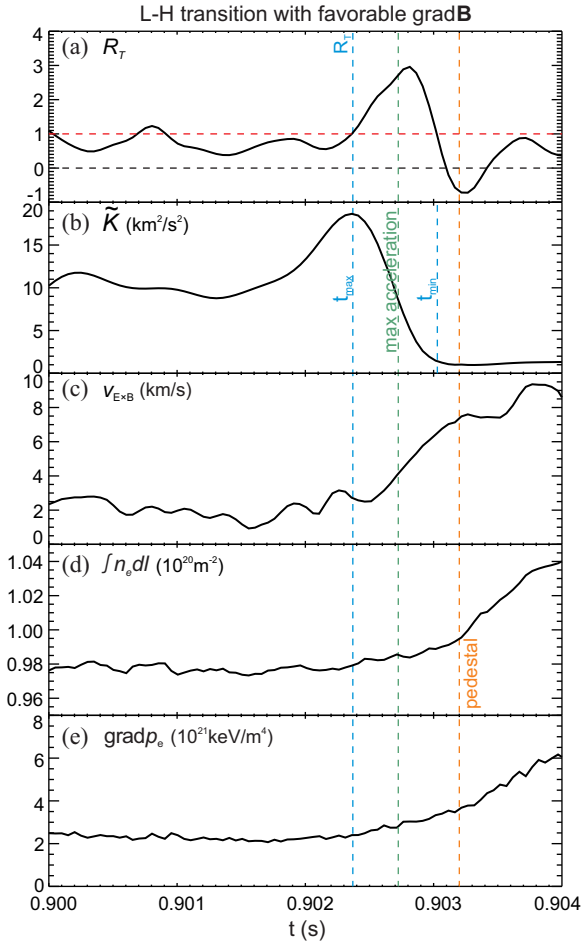

Figure 2. Complete sequence of the L-H transition; a) nonlinear kinetic energy transfer normalized to estimated rate of growth R_T, b) turbulent kinetic energy, c) $\boldsymbol{E} \times \boldsymbol{B}$ drift at the same location, estimated from GPI, TS and ECE, d) line-integrated electron density as measured by FTCI, d) evolution of the total electron pressure gradient at the location of turbulence suppression.

at the time the positive burst in R_T is over, while t_0 denotes a time before the transition when the average level of turbulence is equal to the L-mode value preceding the transition.

While that comparison is mathematically correct and its relationship to R_T is clearly intuitive, it is not optimal from an *experimental* point of view for the following reason. All forms of velocimetry carry a significant level of systematic error, which carries through, and in fact increases in, the estimation of turbulent velocities. Accordingly, very small turbulent velocity fluctuations can be completely overwhelmed by fluctuations of systematic errors, leading to a gross underestimation of the turbulence suppression ratio $\tilde{K}_L/\tilde{K}_{\min}$, as instead of the true $\tilde{K}_{\min}$, the ratio would feature the error level $\delta\tilde{K}$. Therefore, a more reasonable estimate can be achieved by a more direct approach, that is, integrating against time the total amount of transfer,

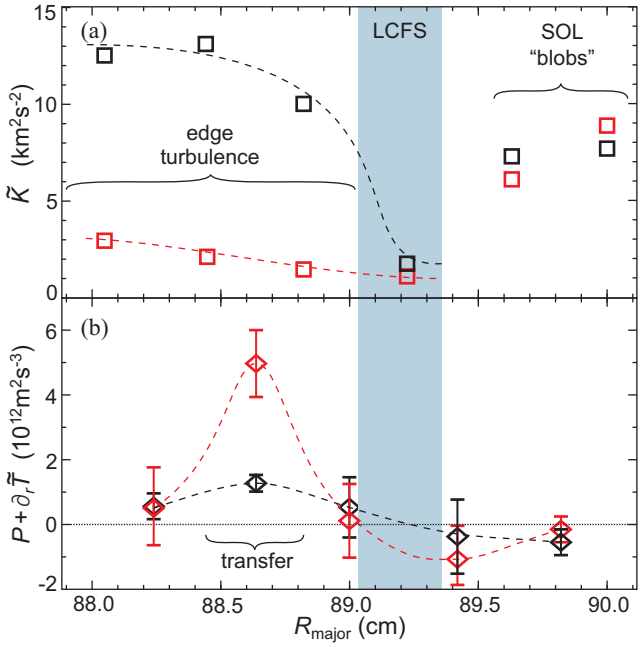

Figure 3. (color online) Radial profiles of key quantities in the L-H transition; a) total turbulent kinetic energy $\tilde{K}$, and b) total kinetic energy transfer $P+\partial_r\tilde{T}$; in L-mode (black) and during the L-H transition (red).

instead of R_T, and compare

$$I_{\rm tr} \equiv \int_{t_{\rm max}}^{t_{\rm min}} P + \partial_r \tilde{T} - \gamma_{\rm eff}\tilde{K}\,{\rm d}t \tag{3}$$

to

$$-\int_{t_{\rm max}}^{t_{\rm min}} \partial_t \tilde{K}\,{\rm d}t = \Delta\tilde{K}; \tag{4}$$

where $t_{\rm min}$ and $t_{\rm max}$ stand for the time instances when the turbulent kinetic energy is minimal and maximal (L-mode level) in the transition, respectively, and $\Delta\tilde{K} = \tilde{K}(t_{\rm max}) - \tilde{K}(t_{\rm min})$ is the absolute loss of turbulent kinetic energy. This correction, due to the lack of division by $\tilde{K}$, is bound to bring the compared linear and nonlinear quantities to a better agreement, as much of the systematic noise can be effectively eliminated.

For the complete consistency of the argument, one further point must be considered. The turbulent kinetic energy, measured using time-delay estimated (TDE) phase velocities of emission features in GPI, is plotted against radial position in Figure 3(a). The graph shows a high level of fluctuation in the edge, becoming smaller in the near scrape-off-layer (SOL), i.e. the open field line region, in which single coherent filaments take over. The comparison between the radial extent of this highly spatially coherent turbulence and that of the production term P in Figure 3(b) is striking. Unsurprisingly, turbulence in its entire radial correlation length is suppressed

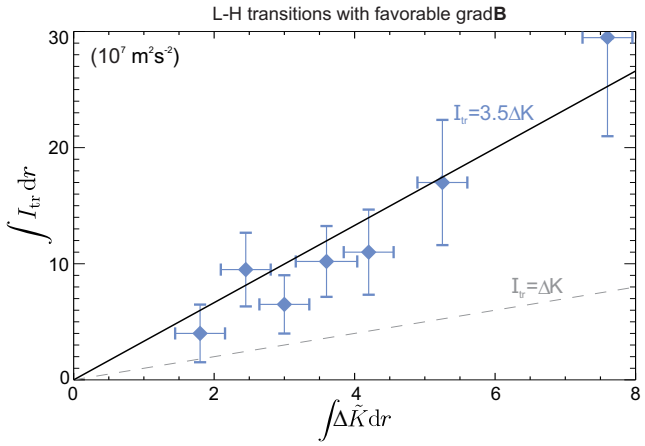

Figure 4. Observed loss of kinetic energy over the entire edge region against the total amount of nonlinear transfer into the zonal flow.

in the initial phase of the transition. At the same time, however, the overwhelming majority of transient zonal flow production occurs in a relatively narrow radial region. Consequently, a quantitative analysis of the total spectrally transferred kinetic energy must consider the full radial extent of the turbulence.

Datasets were therefore restricted to the shots which included at least one correlation length depth of the edge turbulence radially for Figure 4, which shows the total nonlinear transfer in excess of the L-mode level against the observed change of turbulence power. Thus, the diamonds in the figure correspond to $P + \partial_r \tilde{T} - \gamma_{\rm eff} \tilde{K}$ *integrated radially* over the edge and with respect to time between $t_{\rm max}$ and $t_{\rm min}$. As such, the analysis whose result is plotted in the graph addresses all three concerns mentioned above, namely: a) the mismatch between the radial regions of energy transfer and turbulence reduction, b) the underestimation of turbulence reduction due to small fluctuations becoming comparable to or smaller than systematic noise, and c) the limits of integration being restricted to the shortest interval in which turbulence changes are significant.

As can be observed from Figure 4, the total amount of kinetic energy estimated to be transferred from the broadband turbulence to the low frequency flows is still larger than the observed loss of turbulence. The dashed line in the figure represents $\int I_{\rm tr} {\rm d}r = \int \Delta \tilde{K} {\rm d}r$, while the thick solid line is a best fit with a tangent of $\int I_{\rm tr} {\rm d}r / \int \Delta \tilde{K} {\rm d}r = 3.5$; which is a substantial improvement over the discrepancy (up to a factor of ~ 50) the new analysis intended to address. The contributions which the three listed changes to the method of comparison make to this improvement are explained in further detail in the Appendix.

These results strongly corroborate the argument that the lossless nonlinear kinetic energy transfer mechanism is largely responsible for the initial reduction of edge turbulence amplitude, which is thought to lead to the L-H transition. Hence we turn our attention to the path leading to the transition, i.e. to the parametric dependences of nonlinear transfer.

4. Nonlinear transfer in L-mode

As pointed out in the introduction, the ultimate goal of the experiments reported here and similar studies of nonlinear processes in the edge plasma turbulence has been the physically based prediction of the L-H transition threshold. Having reasonably established its direct trigger, i.e. the immediate threshold condition with *edge flows*, one needs to investigate the way plasmas reach this condition. As there are currently no tested models for the parametric dependence of the nonlinear transfer processes in the plasmas leading up to the transition itself, experimental studies are the primary tools at the physicist's disposal. These experiments must, naturally, be conducted in L-mode, with a relatively cold edge, which is thus collisional and which nevertheless has strong turbulence.

It is known that seed E_r shear naturally exists without external heating, and this shear has been demonstrated to increase with heating power. Nonlinearity is expected to follow this trend. In addition, there are a few key macroscale operating parameters – such as plasma density and current, magnetic topology, etc – which are known to have an effect on the transition threshold. Previous studies of nonlinear transfer processes in the edge have shown a difference between the behavior of ZF and GAM.[5] Therefore the L-mode experiments of this section were all performed in the H-mode-unfavorable geometry, since GAM activity is more likely to occur in this setup in Alcator C-Mod[19].

The spectral transfer of fluctuation power is commonly studied in a time averaged sense using cross-bispectral techniques. [3, 5, 13, 24, 25, 26] The transition itself does not have to be achieved or even closely approached in this case, which allows experiments to run in stationary L-mode over a time interval long enough for the measurements of third order spectra. The three-wave coupling terms of primary interest arise from the same convective nonlinearities which stood in the focus of the previous section, and take the form $q\,(\boldsymbol{v}\cdot\nabla q)$, with a Fourier decomposition

$$T_q(f,f_1) = -\mathrm{Re}(\langle \tilde{q}^*(f)\,\tilde{v}_i(f-f_1)\,\partial_i\tilde{q}(f_1)\rangle) \tag{5}$$

for the convective part in the time derivative of $|q|^2$, where z^* is the complex conjugate of the complex number z, and $\tilde{q}(f)$ and $\tilde{\boldsymbol{v}}(f)$ are the Fourier transform of q and $\boldsymbol{v}$, respectively. Generally then, the study of these T_q transfer functions is based on a two-field approach to turbulence, in which the correlations of multiple fluctuation fields are involved in the analysis. For kinetic energy evolution in the edge due to fluctuating shear flows, we are interested in

$$T_v(f,f_1) = -\mathrm{Re}(\langle \tilde{v}_\theta^*(f)\,\tilde{v}_r(f-f_1)\,\partial_r\tilde{v}_\theta(f_1)\rangle)\,. \tag{6}$$

The $\langle . \rangle$ in all the above expressions is an average over a large number of realizations, and can represent ensemble averaging as well as averaging with respect to a slow time variable. For the measurements reported in this section, the brackets represent an average over the small poloidal extent of the GPI view and a time average over a period of several hundred milliseconds. Consequently, on the one hand no time evolution is represented in T_q, but on the other hand one gains the advantages of both being able to reduce errors compared to the time resolved measurements of the previous section and resolving the coupling components by the so-called source (f_1) and target (f) frequencies. This nomenclature is explained by a further advantage of evaluating the two-field transfer function $T_v(f,f_1)$ instead of the more frequently

analyzed bicoherence spectrum, defined as

$$b^2(f, f_1) = \frac{\left|\langle \tilde{v}_\theta^*(f)\, \tilde{v}_r(f - f_1)\, \partial_r \tilde{v}_\theta(f_1)\rangle\right|^2}{\left\langle |\tilde{v}_\theta(f)|^2 \right\rangle \left\langle |\tilde{v}_r(f - f_1)\, \partial_r \tilde{v}_\theta(f_1)|^2 \right\rangle}. \tag{7}$$

The bicoherence is an excellent measure of the strength of phase coupling between components, and as evident from the definition, takes values bounded between 0 and 1, leaving *the* most important questions of energy transfer rate and direction unanswered. The transfer functions are defined such that $T_v(f, f_1)$ takes a positive value (of arbitrary magnitude) if the $\tilde{q}(f)$ Fourier component gains power in the interaction with $\tilde{q}(f_1)$, and a negative one if it loses power. It follows from the definition that for a digitally sampled signal $f \in [0, f_N]$ and $f_1 \in [-f_N, f_N]$ or any consecutive section of length $2f_N$, where f_N is the Nyquist frequency of the sample.

Figures 5(a) and 5(b) show the full two-dimensional transfer function $T_v(f, f_1)$ for an ohmic ($P_{\mathrm{ICRF}} = 0\,\mathrm{MW}$) and a strongly heated ($P_{\mathrm{ICRF}} = 1.6\,\mathrm{MW}$) discharge, respectively. While the function is featureless in the ohmic case, showing no significant transfer into any scale, the heated case exhibits a clear *positive* band at low target frequencies. The fluctuations affected are precisely the ones identified in the previous section as zonal flows, in the $0\,\mathrm{kHz} - 3\,\mathrm{kHz}$ range. Furthermore, the source frequency (f_1) resolution reveals that the nonlinear ZF drive comes from a broad range of frequencies between 5 kHz and 40 kHz, although the estimation of the interaction could potentially be limited near the upper bound of the effective Nyquist frequency $f_N = 50\,\mathrm{kHz}$.

Although the poloidal velocity spectrum exhibits no coherent feature, it is important to note two gaps in the ZF drive spectrum, marked by arrows in Figure 5 around $f_1 = \pm 20\,\mathrm{kHz}$. This is, in fact, the expected frequency range of GAM activity. Thus the ZF does not directly gain power from the spectral space in which GAM should be, nor is there any evidence for changes in the shear flow driving any GAM.

In order to see the overall effect of these nonlinear interactions, it is also instructive to calculate the net frequency resolved transfer function $T_v(f) = \sum_{f_1} T_v(f, f_1)$, which provides a measure of the rate of change of kinetic energy; and the summed bicoherence $B^2(f) = \sum_{f_1} b^2(f, f_1)$, which indicates the total amount of coupling to a given frequency component. However, to give an impression of how far the power pump-out rate is from the ones in transitions, the net kinetic energy transfer can also be normalized completely analogously to the "production term" of the previous section, yielding an effective nonlinear growth rate $\gamma_{\mathrm{NL}}(f) = T_v(f)/\tilde{K}(f)$. Spectra of $T_v(f)/\tilde{K}(f)$ and $B^2(f)$, plotted in Figures 7(a) and 7(b), respectively, both have a peak at the ZF; and the transfer into the other scales is negative on average, as might be expected. The distinction between the two spectra is an important one to make, as it is clear, once again, that no nonlinear driving is detected at the GAM scale, however, the bicoherence spectrum indicates that there is a significant amount of phase coupling at this frequency. The latter will be discussed further in the next section in light of GAM activity, or the lack thereof, in Alcator C-Mod.

All the above nonlinear estimates were calculated from a large number of realizations ($N > 500$) to ensure that bispectra were converged statistically and can thus be considered meaningful. The number of required independent realizations was established in a convergence study. Due to the transfer function taking both positive and negative values, its convergence is more difficult to ascertain rigorously than that of the bicoherence, in which the statistical variance is expected to converge as $1/N$ [27]

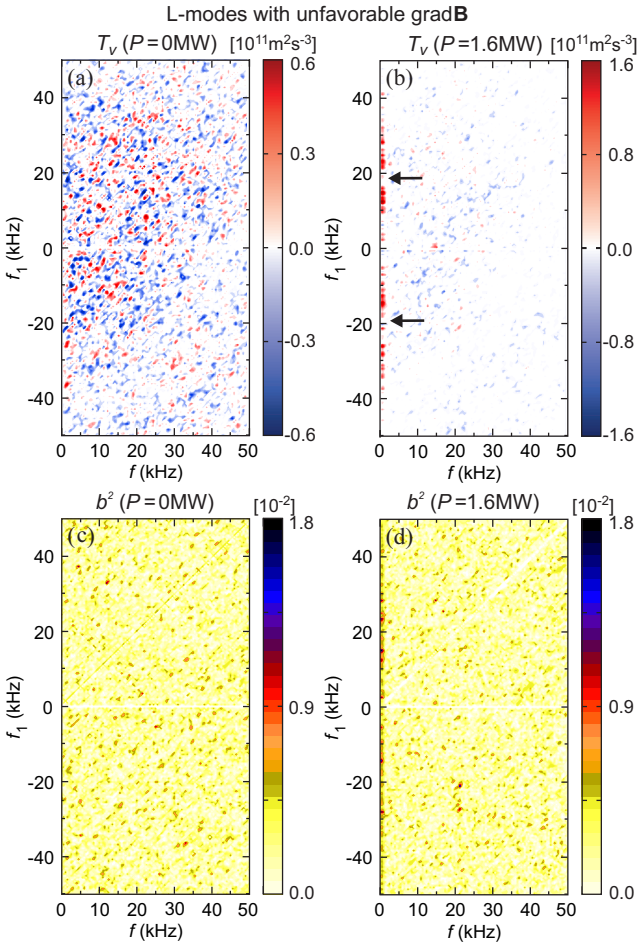

Figure 5. Nonlinear kinetic energy transfer measured by GPI velocimetry for a) ohmic plasma, b) $P_{\mathrm{ICRF}} = 1.6\,\mathrm{MW}$; shown with respective bicoherence spectra for both the c) ohmic and d) heated cases.

owing to the appearance of the modulus and the normalization. The dependence of bicoherence on the number of realizations used in its calculation can then be examined. Convergence occurs in Figure 7 from right to left, as the summed bicoherence at the ZF and the GAM frequencies is plotted against $1/N$. After some initial excursions all show a linear dependence on $1/N$, confirming convergence. From this point the total bicoherence of each feature can be obtained in the limit when N goes to infinity by a linear fit. The limit value of bicoherence at the ZF $B^2_\infty(f = 0.5\,\mathrm{kHz})$ is found to be 0.22 ± 0.03, and that at the GAM $B^2_\infty(f = 20.5\,\mathrm{kHz})$ is 0.10 ± 0.02. Similar values can be found by assuming the baseline of Figure 6(b) to be set by noise alone. This is justified by a random segment of the spectrum, away from both features ($f = 30\,\mathrm{kHz}$), demonstrated to converge to zero within error. Through both methods, one can show that the bispectral signal is reasonably distinguishable from noise by a number of realizations above $N > 280$, as can also be seen in Figure 7 by the excellent linear fit.

The same analysis was performed on the data from a number of experiments, each

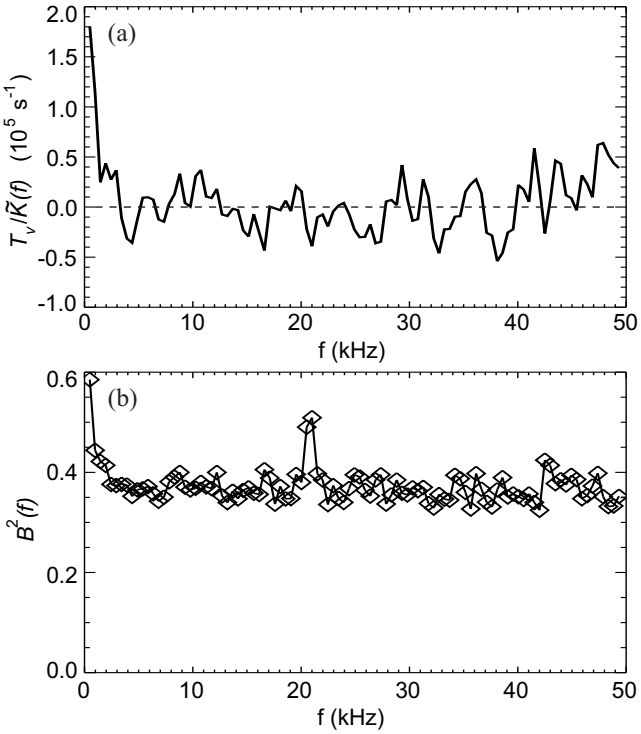

Figure 6. Single frequency measures of nonlinearity; a) net kinetic energy transfer, b) summed bicoherence, showing both ZF and GAM coupling.

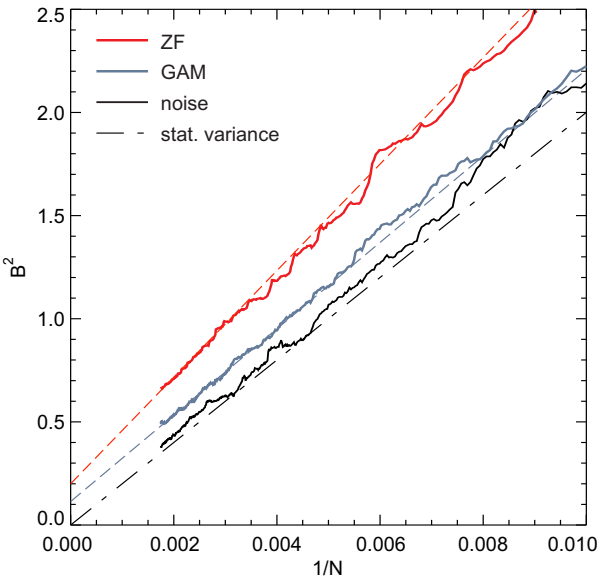

Figure 7. Convergence study performed on the summed bicoherence.

bispectrum tested for convergence. The effective nonlinear ZF growth rates shown in Figure 8 are restricted to those with confirmed convergence. The measured rate of nonlinear zonal flow drive is seen to increase monotonically, indeed near linearly, as ICRF heating is increased. Although data is insufficient at this point to derive any relationship between transfer and plasma density, the densities were restricted for each plasma current to fall within 10% of each other to avoid any ambiguity as to the source of the parametric dependence demonstrated in the figure. In addition to heating power, the transfer rates in Figure 8a are also found to increase with plasma current. This trend is quite sensitive too: the figure shows that a $\sim 30\%$ decrease in I_p means a $\sim 55\%$ decrease in transfer rate, which could only be compensated by a more than twofold increase of the heating power, as evidenced by the difference between the blue and the orange curves.

Motivated by the observation of this trend, the same data is shown reorganized in Figure 8(b), against the total loss power $P_{\rm loss} = P_{\rm RF}^{\rm abs} + P_{\rm OH} - {\rm d}W/{\rm d}t$, where $P_{\rm RF}^{\rm abs}$ is the absorbed power from the ICRF waves, estimated at 80% of the coupled power, W is the stored energy, held steady in the reported experiments, leading to a negligible contribution from this term, and finally $P_{\rm OH}$ is the ohmic heat generated by the plasma current, and thus a major difference between the three sets of measurements. Note in the figure that errors in the measured nonlinear transfer rates are significantly reduced relative to those in L-H transitions due to the long period over which the bispectra are collected. The magnitude of errors can be estimated by making use of the convolution theorem to rewrite $T_v(f)$ as the product of two Fourier series as

$$T_v(f) = {\rm Re}\big(F(v_\theta)^*\, F(v_r \partial_r v_\theta)\big)\,, \tag{8}$$

where F(.) denotes Fourier transformation. For a Gaussian distribution of signal amplitudes, the standard error of Fourier components is $(\sigma_v^2/N)^{1/2}$, equally distributed over the entire spectrum, where σ_v is the variance of the original signal, and N is the number of samples used. Since the steady-state L-mode experiments span a time period approximately 400 times longer than the transition (demonstrated in Fig. 2), the error decreases by about a factor of 20 for a single component. In order to obtain the same frequency-resolution as the fully two-dimensional bispectrum, and cover the range of the ZF ($\sim 2 - 5\,{\rm kHz}$), a few frequency components are added together (the exact number of which depends on the length of the steady-state segment); a conservative estimate gives the final value as the sum of errors, leading to a final improvement in the relative error of a factor ~ 5 still a substantial improvement.

As the measured nonlinear transfer rates in the figure are lined up tightly along a single curve, Figure 8(b) demonstrates the importance of the *cross-field heat flux* in determining the amount of nonlinear coupling and zonal flow drive in the turbulence.

Note that the figure contains only the transfer rates into the low-frequency zonal flow structures, and gives no information on GAM. Standard L-mode discharges on Alcator C-Mod do not exhibit any GAM activity, and so the transfer rates at the GAM frequency are negligible, as expected.

5. Summary and discussion

First, this study presented the first complete measurements of nonlinear zonal flow drive at the L-H transition at a fine temporal and radial resolution from the plasma edge, where the transport barrier forms. Utilizing the full depth of edge turbulence to its radial correlation length and introducing an experimentally robust test of

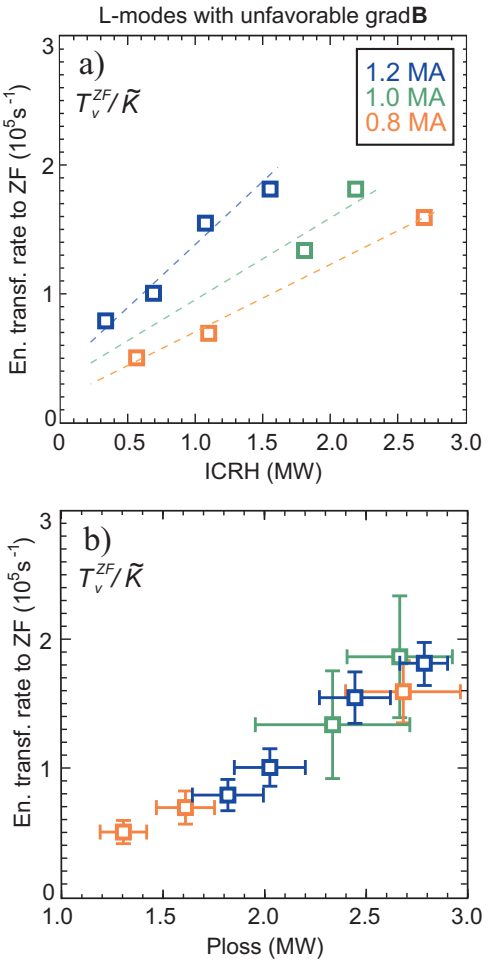

Figure 8. Effective nonlinear growth rates of zonal flows $T_v^{\mathrm{ZF}}/\tilde{K}$ at various plasma currents I_p as a function of a) auxiliary heating power, and b) loss power. Dashed lines are for orientation.

turbulence loss and nonlinear transfer, we resolved a previously reported discrepancy between these two measured quantities. While the total estimated transferred power during transition is still observed to be a factor of $\sim$ 3.5 larger than the turbulence reduction, the new result represents an improvement of more than an order of magnitude. Due to the limited poloidal extent of the observations and the highly asymmetric character of turbulence, this is as good an agreement as can be experimentally expected. Further, mostly simulation based, studies involving the entire three-dimensional structure of edge turbulence are, therefore, highly desirable for the ultimate goals of understanding turbulence reorganization and predicting transitions.

Perhaps more importantly, we reported the first measurements of the L-mode level of nonlinearity in a high performance, diverted tokamak. Our experiments significantly expand the range of auxiliary heating power ($\times$3) over those reported previously from circular, limited tokamak plasmas. In agreement with previous research, results

showed a monotonic increase in the total amount of nonlinear zonal flow drive as the heating power increases. Furthermore, kinetic energy is transferred to zonal flows from the entire detected range of turbulent frequencies ($5\,\mathrm{kHz} - 45\,\mathrm{kHz}$), with the notable exception of expected GAM frequencies. Contrary to previous experiments, it is found that GAM activity, and consequently any nonlinear transfer from turbulence to GAM can be negligible even at moderate levels of heating. In addition, a current scan experiment revealed the nonlinear transfer's parametric dependence on plasma current for the first time. These two new observation taken together make it clear that the parametric dependences of both GAM and ZF transfer warrant further investigation. The accuracy of all nonlinear estimates was tested by studying the statistical convergence of bicoherence spectra. Unlike autopower spectra, the latter did show significant *coupling*, though not transfer, at the GAM frequency.

It should be noted here that GAM fluctuations have only ever been detected in the I-mode regime in Alcator C-Mod. In this case, however, they have been shown to contribute considerably to the dynamics of edge fluctuations.[19] The I-mode, a high energy confinement, low mass confinement regime, is typically produced in the H-mode-unfavorable $\boldsymbol{B} \times \nabla \boldsymbol{B}$ drift topology. Indeed, that is why the L-mode studies of this paper were performed in this geometry, in an attempt to investigate the interplay between GAM and ZF. Due to the currently unknown origin of the so-called weakly-coherent mode (WCM), a characteristic edge fluctuation of I-mode plasmas, imaging studies alone can not study the low frequency flow behavior in this regime. Cross-calibration studies with direct bulk flow measurements via charge exchange spectroscopy are currently conducted and should form the material of later reports. Resolving the competition or interplay between GAM and ZF will also be invaluable for the investigation of L- to I-mode, as well as I-H transitions.

For a complete predictive capability of transition thresholds, future work must also include similar studies in the H-mode favorable magnetic geometry, as well as simulations necessary for providing a fully 3D picture of turbulence. All these should aim to resolve poloidal asymmetry, so we can gain a better understanding of the quantitative analysis shown herein, as well as of the well-known favorable/unfavorable asymmetry.

Acknowledgments

The authors would like to thank the Alcator C-Mod team of students, scientists, engineers and technical staff for making the experiments possible. This material is based upon work supported by the U.S. Department of Energy, Office of Science, under Award Numbers DE-SC-0008689 and DE-FC02-99ER54512.

Appendix

The present study provided an improved comparison of the loss of turbulence kinetic energy to nonlinear transfer over a previous publication. The contributions which the three listed changes to the method of comparison make to this improvement are as follows.

Firstly, upon selection of experiments in which the full radial correlation length of edge turbulence is covered in GPI views, a least squares fit yields a tangent of $m = \int_{t_0}^{t_m} (R_T - 1)\gamma_{\mathrm{eff}}\,\mathrm{d}t / \ln\left(\tilde{K}_{\mathrm{L}}/\tilde{K}_{\mathrm{m}}\right) \approx 33.7$. The error in the measurement of

kinetic energy is $\delta\tilde{K} \approx 1\,\mathrm{km}^2/\mathrm{s}^2$, while the measured turbulent kinetic energy right at the collapse of edge turbulence is also $\tilde{K}_\mathrm{m} \approx 1\,\mathrm{km}^2/\mathrm{s}^2$. Due to the fact that the measured kinetic energy is a quadratic form of the velocity measurement, errors of this magnitude are systematically positive. In other words, this result is consistent with the systematic error dominating the empirical values of $\tilde{K}$ at the end of the transition. Even if the mean $\tilde{K}$ in the fully quenched state of turbulence is in fact $\tilde{K}_\mathrm{m} = \delta\tilde{K}$, this causes a minimal systematic shift of $\ln 2$ towards smaller values (which can be as much as a 50% shift), and a relative error of $\delta\tilde{K}/\tilde{K} \approx 0.6$. If this shift were systematically applied to the whole range of data a tangent of $m' = 28.7$ would be obtained. In contrast, using $\Delta\tilde{K}$ has the advantage of introducing a total error of $\delta\Delta\tilde{K} = \delta\tilde{K}_\mathrm{L} + \delta\tilde{K}_\mathrm{m} \approx 1\,\mathrm{km}^2/\mathrm{s}^2 + 1\,\mathrm{km}^2/\mathrm{s}^2$, resulting in a relative error of only $\delta\Delta\tilde{K}/\Delta\tilde{K} \approx 0.2$, and any shift due to systematic overestimation of collapsed turbulence is 10% in the worst case.

Secondly, similarly to the error propagation in the measure of turbulence loss, the large relative error in kinetic energy at the collapse of turbulence $\delta\tilde{K}/\tilde{K}_\mathrm{m} \lesssim 1.0$ is inherited in R_T *as relative error*, i.e. at the *end* (but not the beginning) of the transition $\delta R_T/R_T \approx \delta P/P + \delta\tilde{K}/\tilde{K} \lesssim 1.0$. This has two consequences: 1) the integral of R_T will carry a large error due to the error of the integrand; 2) if the upper limit of the integration is determined by the evolution of R_T, as in [10], there will be an additional error due to the uncertainty in determining the integration limit. In contrast, the expression in (3) reduces both effects, as the absolute error in the integral (taking a representative case) is $\delta(P - \gamma_\mathrm{eff}\tilde{K}) \approx 1.6 \times 10^5\,\mathrm{km}^2/\mathrm{s}^2 + 5 \times 10^4\,\mathrm{km}^2/\mathrm{s}^2$, i.e. approximately 30%. Selecting the limits by the evolution of $\tilde{K}$ invariably yielded a shorter integration interval, with some portions of the integrand with *large values* – but also *large errors* – excluded. A fit in this case provides a tangent of $I_\mathrm{tr}/\Delta\tilde{K} = 15.4$.

Finally, the layer in which the nonlinear transfer is significant is much narrower ($\lesssim 3.8\,\mathrm{mm}$) than the region in which turbulence exists and is reduced in the transition ($\sim 1.5\,\mathrm{cm}$). Once a summation is performed in the radial direction over the entire visible range of edge turbulence, the tangent gains the value quoted in the main text of the paper, i.e. $\int I_\mathrm{tr}\mathrm{d}r / \int \Delta\tilde{K}\mathrm{d}r = 3.5$.

References

[1] I. H. Hutchinson, R. Boivin, F. Bombarda, P. Bonoli, S. Fairfax, C. Fiore, J Goetz, S. Golovato, R. Granetz, M. Greenwald, et al. *Phys. Plasmas*, 1:1511, 1994.

[2] G. R. Tynan, C. Holland, J. H. Yu, A. James, D. Nishijima, M. Shimada, and N. Taheri. *Plasma Phys. Controlled Fusion*, 48:S51, 2006.

[3] M. Xu, G. R. Tynan, C. Holland, Z. Yan, S. H. Muller, and J. H. Yu. *Phys. Plasmas*, 16:042312, 2009.

[4] P. Manz, M. Ramisch, and U. Stroth. *Phys. Rev. Lett.*, 103:165004, 2009.

[5] M. Xu, G. R. Tynan, P. H. Diamond, P. Manz, C. Holland, N. Fedorczak, S. C. Thakur, J. H. Yu, K. J. Zhao, J. Q. Dong, et al. *Phys. Rev. Lett.*, 108:245001, 2012.

[6] L. Schmitz, L. Zeng, T. L. Rhodes, J. C. Hillesheim, E. J. Doyle, R. J. Groebner, W. A. Peebles, K. H. Burrell, and G. Wang. *Phys. Rev. Lett.*, 108:155002, 2012.

[7] P. Manz, G. S. Xu, B. N. Wan, H. Q. Wang, H. Y. Guo, I. Cziegler, N. Fedorczak, C. Holland, S. H. Müller, S. C. Thakur, M. Xu, K. Miki, P. H. Diamond, and G. R. Tynan. *Phys. Plasmas*, 19:072311, 2012.

[8] G. R. Tynan, M. Xu, P. H. Diamond, J. A. Boedo, I. Cziegler, N. Fedorczak, P. Manz, K. Miki, S. Thakur, L. Schmitz, et al. *Nucl. Fusion*, 53:073053, 2013.

[9] Z. Yan, G. R. McKee, R. Fonck, P. Gohil, R. J. Groebner, and T. H. Osborne. *Phys. Rev. Lett.*, 112:125002, 2014.

[10] I. Cziegler, G. R. Tynan, P. H. Diamond, A. E. Hubbard, J. W. Hughes, J. H. Irby, and J. L. Terry. *Plasma Phys. Control. Fusion*, 56:075013, 2014.

[11] E. Kim and P. H. Diamond. *Phys. Rev. Lett.*, 90:185006, 2003.
[12] K. Hallatschek. *Phys. Rev. Lett.*, 93:065001, 2004.
[13] C. Holland, G. R. Tynan, R. J. Fonck, G. R. McKee, J. Candy, and R. E. Waltz. *Phys. Plasmas*, 14:056112, 2007.
[14] K. Miki, P. H. Diamond, Ö. D. Gürcan, G. R. Tynan, T. Estrada, L. Schmitz, and G. S. Xu. *Phys. Plasmas*, 19:092306, 2012.
[15] F. Wagner, G. Becker, K. Behringer, D. Campbell, A. Eberhagen, W. Engelhardt, G. Fussmann, O. Gehre, J. Gernhardt, G. v. Gierke, et al. *Phys. Rev. Lett.*, 49:1408, 1982.
[16] P. H. Diamond, S. Itoh, K. Itoh, and T. S. Hahm. *Plasma Phys. Control. Fusion*, 47:R35, 2005.
[17] N. Winsor, J. L. Johnson, and J. M. Dawson. *Phys. Fluids*, 11:2448, 1968.
[18] I. Cziegler, J. L. Terry, J. W. Hughes, and B. LaBombard. *Phys. Plasmas*, 17:056120, 2010.
[19] I. Cziegler, P. H. Diamond, N. Fedorczak, P. Manz, G. R. Tynan, M. Xu, R. M. Churchill, A. E. Hubbard, B. Lipschultz, J. M. Sierchio, et al. *Phys. Plasmas*, 20:055904, 2013.
[20] S. B. Pope. *Turbulent Flows*. Cambridge University Press, Cambridge, UK, 2000.
[21] C. Hidalgo, C. Silva, M. A. Pedrosa, E. Sanchez, H. Fernandez, and C. Varandas. *Phys. Rev. Lett.*, 83:2203, 1999.
[22] P. Manz, M. Xu, N. Fedorczak, S. C. Thakur, and G. R. Tynan. *Phys. Plasmas*, 19:012309, 2012.
[23] G. Y. Park, S. S. Kim, T. Rhee, H. Jhang, P. H. Diamond, and X. Q. Xu. In *Proc. 25th IAEA Fusion Energy Conference (St. Petersburg, Russia)*, pages TH/8–1, 2014.
[24] C. P. Ritz and E. J. Powers. *Physica D*, 20:320, 1986.
[25] C. P. Ritz, E. J. Powers, and R. D. Bengtson. *Phys. Fluids B*, 1:153, 1989.
[26] Y. Kim, R. D. Durst, R. J. Fonck, A. Ware, and P. W. Terry. *Phys. Plasmas*, 3:11, 1996.
[27] Y. Nagashima, S.-I. Itoh, M. Yagi, K. Itoh, A. Fujisawa, K. Hoshino, K. Shinohara, K. Uehara, Y. Kusama, A. Ejiri, and Y. Takase. *Rev. Sci. Instrum.*, 77:045110, 2006.